RSC Advances

ROYAL SOCIETY OF CHEMISTRY

www.rsc.org/advances

Disparate impact between two types of GMI effect definition for DC Joule-heating annealed Co-based microwires

Si-Da Jiang [a], Da-Wei Xing[a], Wei-Dong Fei[a], Jing-Shun Liu[b], Hong-Xian Shen[a], Wen-Bin Fang[a,c], Jian-Fei Sun[*a]

[a] *School of Materials Science and Engineering, Harbin Institute of Technology, Harbin 150001, People's Republic of China.*

[b] *School of Materials Science and Engineering, Inner Mongolia University of Technology, Hohhot 010051, People's Republic of China*

[c] *School of Materials Science and Engineering, Harbin University of Science and Technology, Harbin 150080, P. R. China.*

Abstract

Based on a comprehensive study of progressive DC Joule-heating annealing (DJA) on giant magneto-impedance (GMI) properties of melt-extracted amorphous microwires，we systematically analysis the different mechanism for two types of GMI effect definition. Experimental results show that DJA can improve the GMI response characteristics and magnetic field sensitivity (MFS) effectively for both definitions，but $\Delta Z/Z_0$ enhances much higher than $\Delta Z/Z_{max}$ of the as-cast wires. At 20 MHz, the maximum GMI ratios as respectively denoted by $\Delta Z/Z_0$ and $\Delta Z/Z_{max}$ of DJA microwires enhance to 582.59% and 639.13%, while the values for as-cast wires are 69.09% and 520.48% respectively. Meanwhile, the MFS (ξ_{max}) and equivalent magnetic anisotropy field (H_k) increase to 1346.4%/Oe ($\Delta Z/Z_0$), 2927.9%/Oe ($\Delta Z/Z_{max}$) and 1.1Oe, respectively. These significant effects of GMI properties as denoted by Z_0 are mainly attributed to the change of resistivity (ρ_{dc}) for amorphous microwires

[*] Corresponding author: jfsun@hit.edu.cn (*Jianfei Sun*).

induced by DJA. Revealing this mechanism of different effect can also result in developing micromagnetic field sensor, especially for geomagnetic sensor applications (~±1.0 Oe).

Introduction

Recently, melt-extracted amorphous microwires have attracted much attention due to their variously potential industrial applications, especially as giant magneto-impedance (GMI) sensor elements for detecting weak magnetic fields.[1–4] Compared with other fabrication techniques including rotating-water and glass-covered spinning, melt-extracted microwires without glass-covered coating exhibit a higher cooling rate, which resulting in better mechanical and magnetic properties, such as superior soft magnetic properties and large fracture strengths. These excellent performances promote the melt-extracted microwires more suitable for applied in electronic package and magnetic sensors, especially for GMI sensor elements. From the previous works based on a great deal of related experiments conducted by our group, the parameters of melt-extraction can be accurately and effectively controlled, thus Co-based melt-extracted microwires with excellent GMI properties can be easily fabricated used for designing sensors for detecting micromagnetic fields.[5-7]

Key theory of GMI effect is therefore ascribed to the well-known skin effect, which means the AC current flows only in the outer region of the magnetic amorphous wires at high frequency; on the other hand, with a higher frequency of AC, the effective conducting cross-section is almost limited. Remarkably, impedance of amorphous

wires will sharply change when applied extra axial magnetic field (H_{ex}), which influences the circumferential magnetization process under specific conditions. Skin effect is determined by the skin depth, as denoted by $\delta = (\rho/\pi f \mu_\varphi)/2$, where μ_φ is the circumferential direction magnetic permeability of the microwires, ρ is the electrical resistivity and f is the AC frequency.[8-12] In general, there are two classic types of definition for quantitively evaluating GMI effect appeared in previous reports: one is quantitatively measured by the Z_0 (H_{ex}=0), the GMI ratio as denoted by $\Delta Z/Z_0$ is defined by Eq. 1 as reported in Ref. [13]; the other is based on Z_{max} (H_{ex}=max), the GMI ratio, as denoted by $\Delta Z/Z_{max}$, is defined by Eq. 2 as reported in Ref. [14].

$$\frac{\Delta Z}{Z_0}(\%) = \left[\frac{Z(H_{ex}) - Z(H_0)}{Z(H_0)}\right] \times 100\% \quad (1)$$

$$\frac{\Delta Z}{Z_{max}}(\%) = \left[\frac{Z(H_{ex}) - Z(H_{max})}{Z(H_{max})}\right] \times 100\% \quad (2)$$

So in terms of these two specific definitions, GMI sensor own several design ideas to apply for different work environments.

Commonly, melt-extracted microwires have relatively large residual inner stress, which reduce their magnetic properties, also GMI performances. Based on the privious reports, the GMI response of sensitive materials mainly can be optimized through proper post-processing treatments. Lots of work has been done for enhancing GMI performance by annealing treatments: L. V. Panina et al.[15] firstly reported that effect of tension annealed (TA) on amorphous microwires, which average change rate of voltage can reach 50%/Oe at 10 MHz. Moron et al.[16] reported that vacuum annealing (VA) Fe-based nanocrystalline microwires enhanced magnetic properties,

GMI ratio increased from 1% of as-cast to 5% after VA treatment. Zhou et al.[17] observed that the effect of AC Joule-heating (AC) for melt-spun CoFeSiB amorphous ribbon on GMI property, and $[\Delta Z/Z_0]_{max}$ enhanced to about 180% at 900 kHz for 30 min with AC current density 2.8×10^7 A/m^2. V. Zhukova et al.[18] reported that DC current annealing (DCA) with or without DC axial magnetic field can significantly influence magnetic properties of glass-coated microwires, and the obvious longitudinal magnetic anisotropy generated by the combined effects of the magnetic field and internal stresses arising from the coating during annealing. K. R. Pirota et al.[19] found that DC Joule annealing (DJA) induced a short-range order relaxation hence distinctly improved the soft magnetic properties of Co-based glass-coated microwires and $[\Delta Z/Z_{max}]_{max}$ at 15 MHz of nearly about 600% for annealing conditions (as included for 10 min annealing and 70 mA). Regretfully, we attempt to make a complete list or comparison of post-treatment due to its diversity, and according to the above mentioned reports and the wire shape, Joule-heating annealing probably is a suitable method for post-processing of melt-extracted wires. Above all of these, researchers usually focus on one type definition and try to establish relationship between GMI effect and circumferential magnetic permeability.

In this paper, the effect mechanism of post-treatment on amorphous microwires will be systematically studied based on two types of definition. We attempt to through quantitative analysis the impedance of $Co_{68.15}Fe_{4.35}Si_{12.25}B_{14.25}Zr_1$ melt-extracted amorphous microwires (herein, take it as the research samples) with progressive DC Joule-heating annealing (DJA) to reveal different change mechanism induced by

annealing of two types of GMI effect definition. Generally, the current annealing applied on different wires for the annealing time was under 600s. Differently, we choose one wire to anneal by step mode and the total annealing time could reach 50 min, we have introduced detailed in our published paper.[20] This modified DJA effectively avoid the experimental error and the nonuniform of different microwires during the measurements, and we would obtain the optimal magnetic properties, especially for the GMI ratio and MFS of sensitive materials. Moreover, H_k enhanced to ~1 Oe is an important index for application-oriented GMI sensor.

Experimental

Mother alloy ingot with nominal composition of $Co_{68.15}Fe_{4.35}Si_{12.25}B_{14.25}Zr_1$ (in at.%) was firstly prepared by arc-melting in pure argon and copper mold casting methods. During melt-extraction process, the mother alloy in Boron Nitride (BN) crucible was re- melted by induction coil and extracted by the edge of a high-speed rotating Cu wheel in purified argon and the schematic diagram is also shown in our previous reports.[20]

The obtained wires possess the diameters ranging from 20 to 100 μm and saturated magnetostriction with nearly a small negative value (nearly $|\lambda_s| \leq 10^{-6}$).[21] The uniform and continuous wire with diameter of ~42 μm was selected and post-processed by DJA, which currents ranging from 60 mA (nearly equal to 4.33×10^7 A/m^2) to 120 mA (nearly equal to 8.66×10^7 A/m^2), step value was set as 20 mA and annealing time is 600 s for each stage.[20] The impedance of wire was measured on an Agilent 4294A precision impedance analyzer, which frequencies of driving current were varied from

0.1~20 MHz and amplitude of driving current was kept at 20 mA, resistivity was measured by Agilent 4339B and the length of sample was 26 mm when connected by Cu clamping apparatus. And it was placed in a pair Helmholtz coils paralleling to the axis of the wires for avoiding the disturbance of geomagnetic field. The DC magnetic field sensitivity ξ of GMI can be expressed as follows:

$$\xi_{Z_0}(\%/Oe) = \frac{d[\Delta Z/Z_0]}{dH_{ex}} \quad (3)$$

$$\xi_{Z_{max}}(\%/Oe) = \frac{d[\Delta Z/Z_{max}]}{dH_{ex}} \quad (4)$$

where Z (H_{ex}) denotes impedance of the axial applied external field, H_{ex} was supplied by Helmholtz coils by using a step-like changing current up to 100 Oe, Z (H_{max}) indicates the final impedance in a maximum magnetic field of 100 Oe.

The structure information of as-cast wires was examined by X-ray diffraction with Cu Kα radiation (XRD, Rigaku D/max-γ B), scanning electron microscope (SEM, Hitachi S-4700). In addition, the microstructure of as-cast and annealed wires was examined by high-resolution transmission electron microscopy (HRTEM, Tecnai G2F30) and the steps for HRTEM sample preparation are shown in Ref. [22]. The measurement of magnetic properties was carried out on a vibrating sample magnetometer (VSM, Lake Shore 7410).

Results and discussions

Fig.1 shows XRD pattern and SEM image of as-cast microwires. XRD pattern displays a broad diffused diffraction maximum. This evidence directly indicates that the as-cast mainly consists of amorphous phase. The diameter of wire is ~42μm and

the surface of the wire is quite smooth as shown in the SEM image of Fig.1. Almost no macro Rayleigh wave defect from the SEM observation. However, there exists groove on the wire which is induced due to the contact surface between melt puddle and quenching Cu wheel during the course of fabrication.[20] Relatively, more smooth and no obvious defects conduce to achieve an excellent GMI property.[23,24]

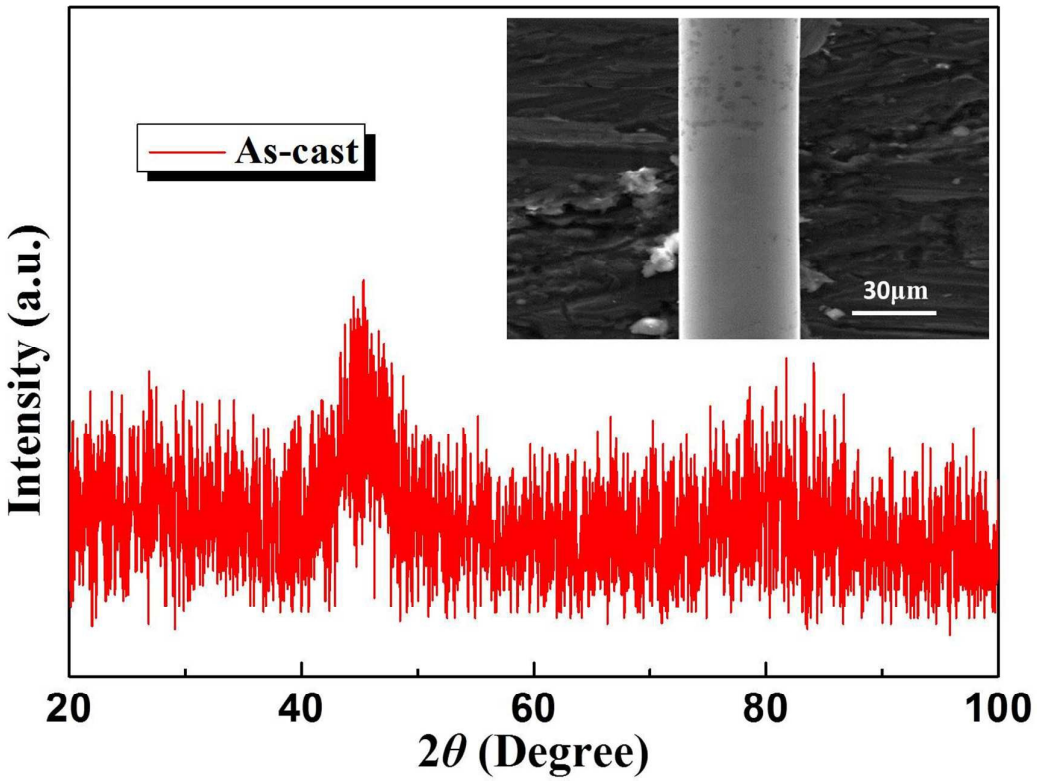

Fig. 1 XRD pattern and the inset displays SEM image of as-cast microwire.

Then we measured the GMI effects for both as-cast and post-treatment wires. Fig. 2 describes the GMI ratio profiles of as-cast and variation tendency of DJA-ed microwires change with H_{ex} by different current intensity range of 60~120 mA at 20 MHz, concentrated on the different definitions by Eqs. 1 & 2, respectively. Noted that the ratio defined by $\Delta Z/Z_0$ is enhanced when the annealing current intensity increased from 60 (nearly equal to 4.33×10^7 A/m^2) to 80 mA (nearly equal to 5.76×10^7 A/m^2)

and then reduced as continue to increase current density. And the $[\Delta Z/Z_0]_{max}$ can achieve 582.59% at 80 mA and nearly enhance 8.4 times comparing with as-cast wires of 69.09%. Correspondingly, the tendency of GMI ratio defined by $\Delta Z/Z_{max}$ expresses similar law of increased at first and then decreased with the annealing current increase, but the $[\Delta Z/Z_{max}]_{max}$ improved from 520.89% of as-cast wire to 639.13% of after 60 mA annealing. The insets clearly show the GMI ratios at weak externally magnetic field. Then we can therefore evaluate GMI effect at different annealing current density stages by different definitions, which show various characteristics for designing new sensors. At H_{ex} = 0 Oe, all curves show different starting points for $\Delta Z/Z_{max}$ as shown in inset of Fig. 2b, and on the contrary these curves show the same star value for $\Delta Z/Z_0$ in inset of Fig. 2a.

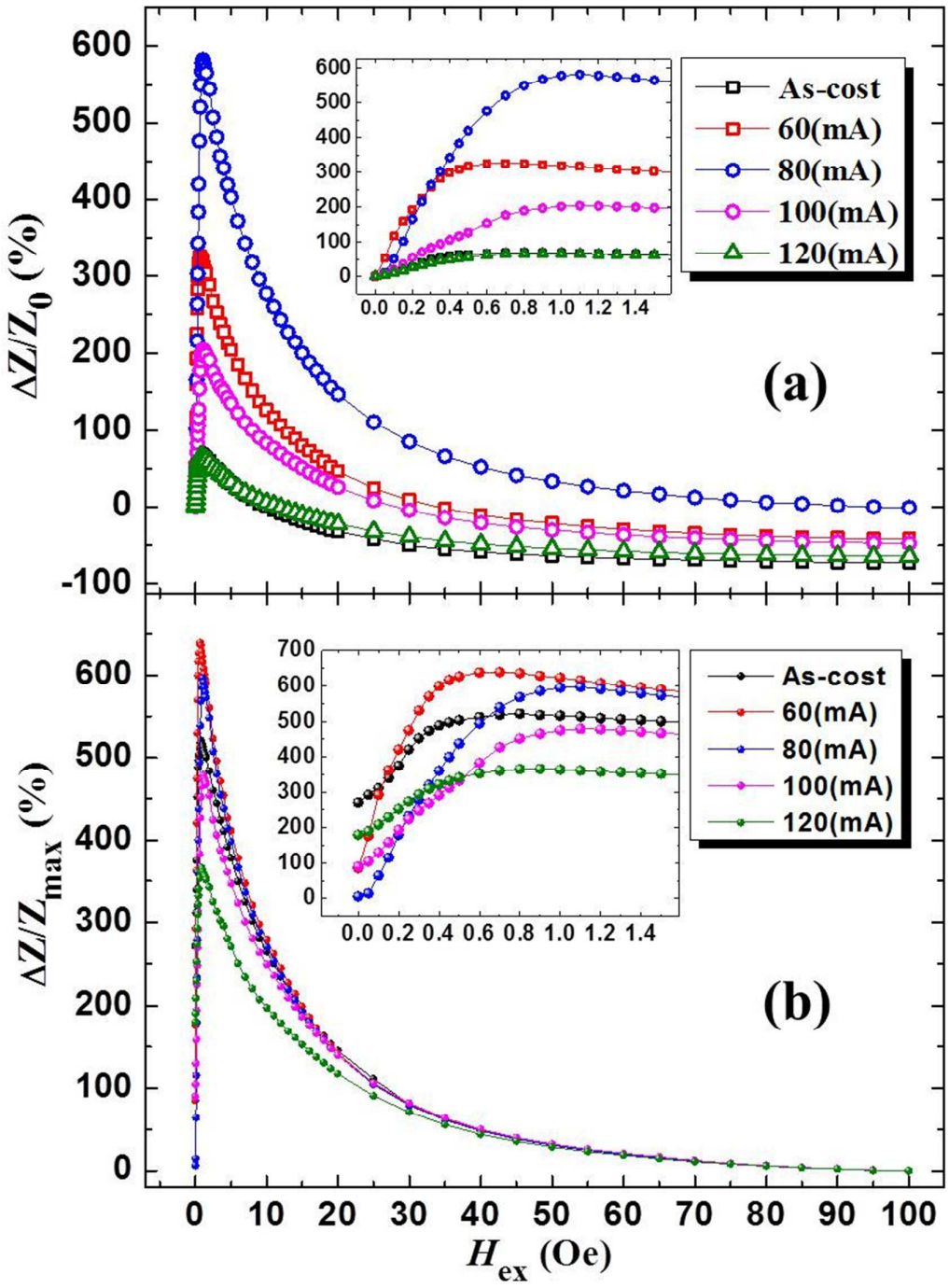

Fig. 2 GMI ratio curves of as-cast and variation tendency of DJA-ed microwires change with H_{ex} by different current intensity range of 60~120 mA at 20 MHz, (a) defined by Z_0 (H_{ex} = 0 Oe) and enlarged inset shows the tendency on weak externally magnetic field (0~1.5 Oe) and (b) definition by Z_{max} (H_{ex} = 100 Oe).

Obviously, we confirm that the better parameters of DJA method for obtaining quantitative values of GMI effects according to Fig. 2, which are 80 mA and 60 mA for $\Delta Z/Z_0$ and $\Delta Z/Z_{max}$, respectively, as shown in Fig. 2a and 2b. Thus we show the field dependence of GMI curves in detail at selected frequencies from 0.1-20 MHz at annealing stage (a) 80 mA for 600 s ($\Delta Z/Z_0$) and (b) 60 mA for 600 s ($\Delta Z/Z_{max}$) of the single microwire in Fig. 3. Basically, GMI ratio curves sequentially increase with different driving frequencies for both definitions in Fig. 3a and b. At $f \geq 13$ MHz, the value of ratio exceeds 500% after 80 mA annealing for $\Delta Z/Z_0$ definition as shown in inset of Fig. 3a. Threshold value of driving frequency will decrease to 5 MHz for 60 mA ($\Delta Z/Z_{max}$). GMI profiles illustrate the high sensitivity of impedance for $\Delta Z/Z_0$ definition when $H_{ex} \leq 1.1$ Oe as seen in inset of Fig. 3a and for $\Delta Z/Z_{max}$ definition when $H_{ex} \leq 0.7$ Oe. All the GMI curves show exhibit a single-peak feature at $f \geq 0.1$ MHz for both GMI definitions. This remarkable behavior has potential applications of GMI sensors applied for weak field detection,[14] espeically for requiring small bias fields and high sensitivity such as bio-magnetic and geomagnetic detection. Another noticeable feature is that GMI curves at different frequencies almost show linear changes to the magnetic field from 1.1~50 Oe for $\Delta Z/Z_0$ definition and 0.7~40 Oe for $\Delta Z/Z_{max}$ definition as shown in Fig. 3a and Fig. 3b, respectively, which displays a wider range of external fields for detecting a larger bias field with high sensitivity. Therefore, high sensitivity to weak magnetic field and linear response to larger magnetic field make this post-treated microwire can be exploited for double functional GMI sensors applications.[24]

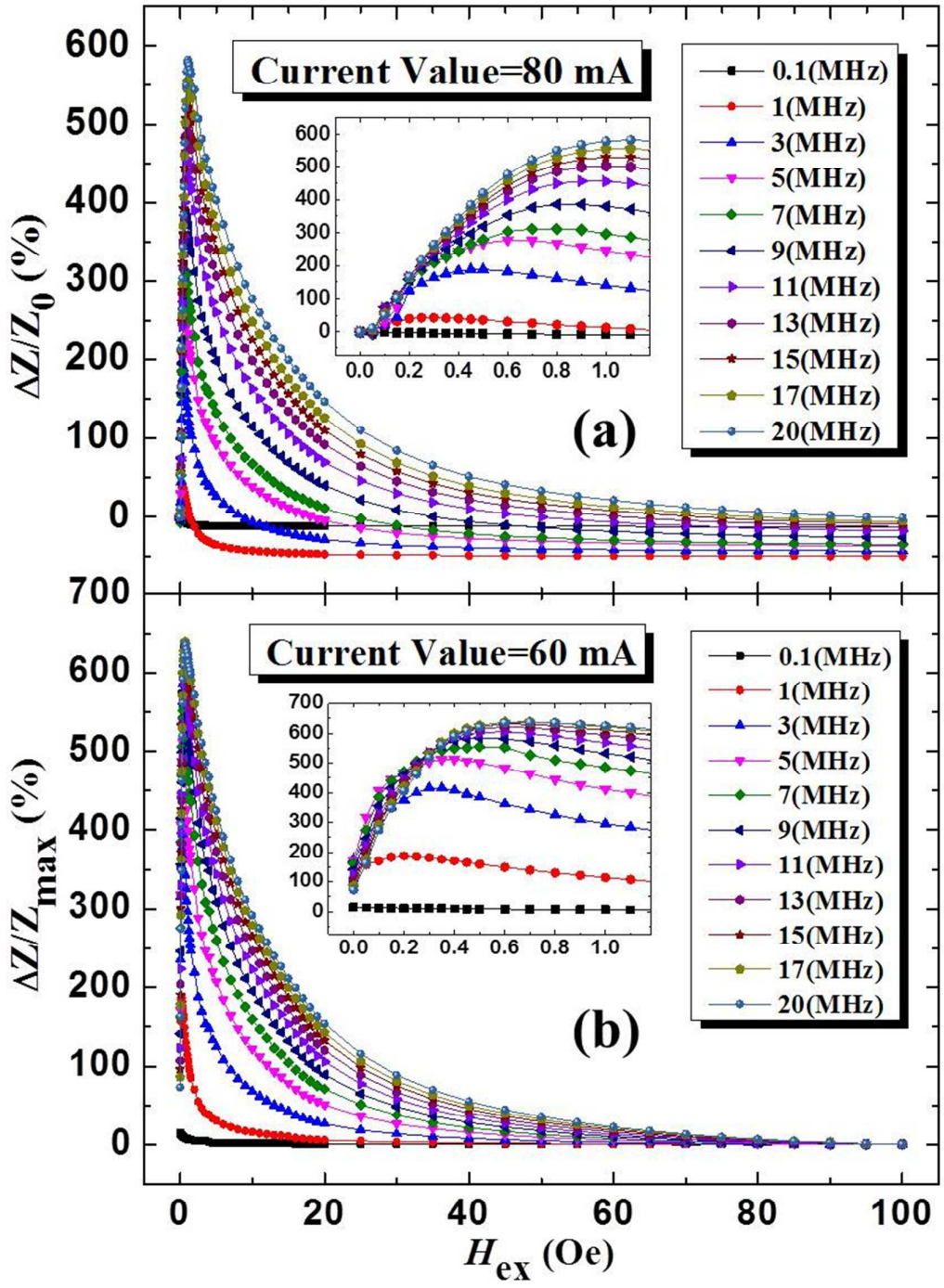

Fig. 3 Field dependence of GMI profiles at selected frequencies between 0.1~20 MHz in different annealing stages (a) 80 mA for 600 s ($\Delta Z/Z_0$) and (b) 60 mA for 600 s ($\Delta Z/Z_{max}$) of the single microwire. The magnified insets of the curve linear increase field response at working ranges (0~1.1 Oe).

Magnetic field sensitivity decides the intrinsic response speed of GMI sensitive material, so it acts as the decisive designed parameter for sensor. Fig. 4 illustrates respectively magnetic field sensitivity (ξ_{max}) and $[\Delta Z/Z]_{max}$ as functions of annealing current densities by different definitions. From above images, the maximum GMI ratio $[\Delta Z/Z]_{max}$ (%) and ξ_{max} %/Oe obviously changing with the amplitudes of annealing current and they have similar salient and takes on a jumping tendency. After 60 mA annealing, $\xi_{Z_{max}}$ and $[\Delta Z/Z_{max}]_{max}$ reach 2927.9%/Oe and 639.13%, respectivly, meanwhile the ξ_{Z_0} and $[\Delta Z/Z_0]_{max}$ get the largest value of 1346.4%/Oe and 582.59% at 80 mA annealing, respectively. These magnetic field sensitivity $\xi_{Z_{max}}$ and ξ_{Z_0} are bigger the most amorphous wires mentioned in Ref. [1]. Measured by different modes, ξ and $\Delta Z/Z$ possess unlike starting threshold and dramatically decrease when surpassing the threshold value. So, we obtained excellent and specific performance of ξ corresponding to driving frequency at diverse threshold in Fig. 5. Both them have a sharp enhance tendency at $f \leq 5$ MHz, then decline and almost keep constant. In all tests of frequency domain, all values of $\xi_{Z_{max}}$ are higher than that of ξ_{Z_0}.

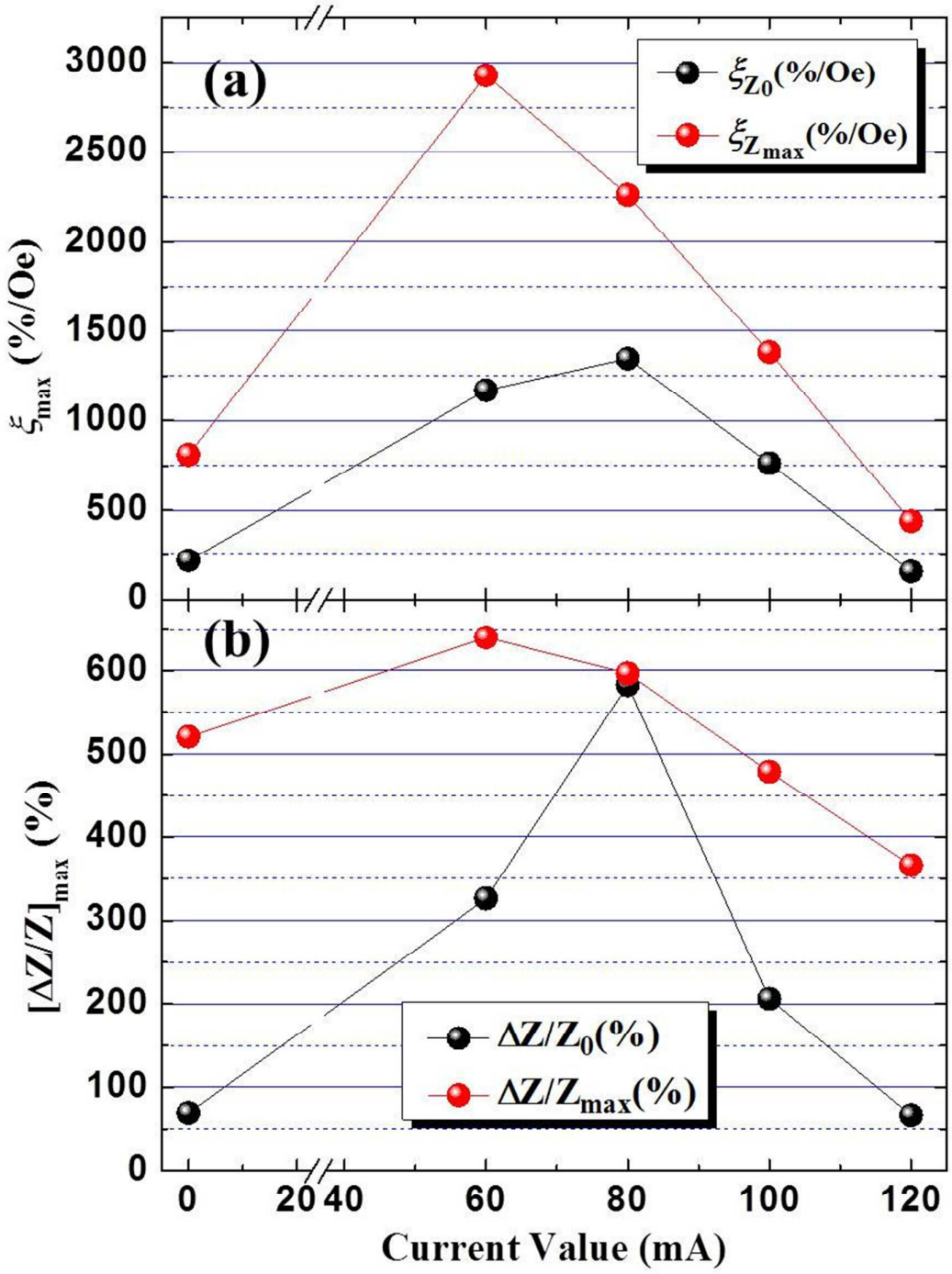

1

2 **Fig. 4** (a) Magnetic field sensitivity ξ_{max} and (b) GMI ratio $[\Delta Z/Z]$ of H_k by different definition

3 mode change with different annealing current density.

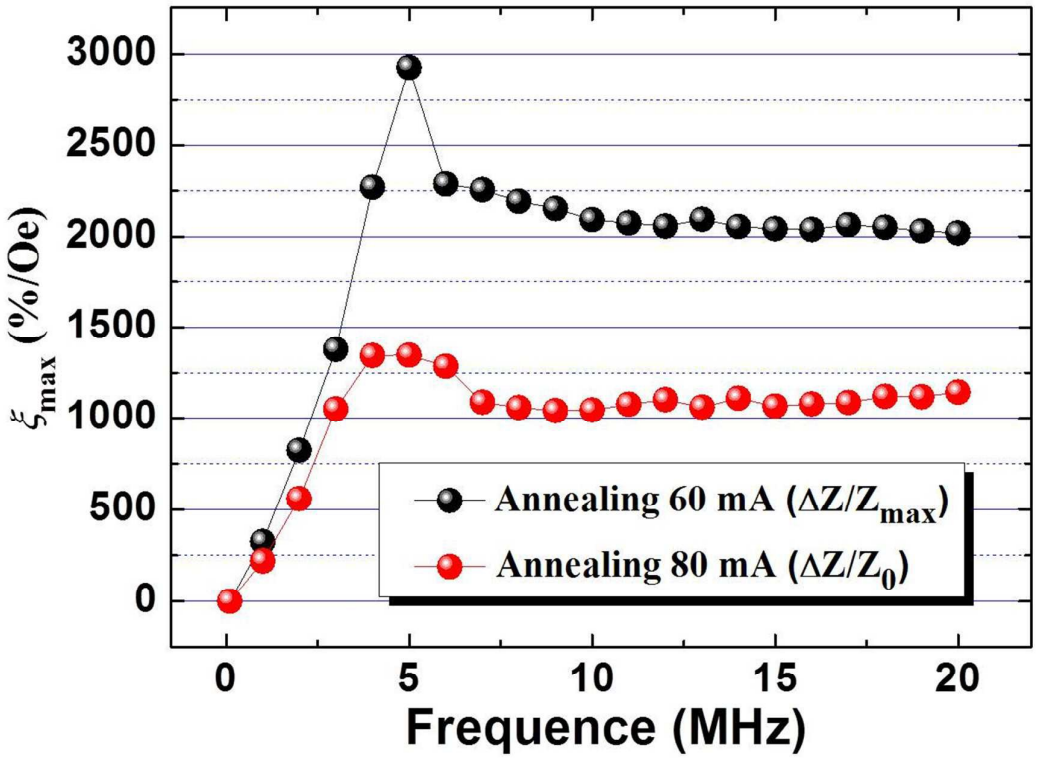

Fig. 5 Magnetic field sencitivity ξ_{max} of ideal annealing stage depend of frequency defined by Z_{max} and Z_0.

The working magnetic field and frequency are equally important factors for sensor application, usually for weak field detecting sensor, and the working field range means the equivalent anisotropy field H_k, which is the corresonding magnetic field of maximum GMI ratio. Fig. 6 shows equivalent anisotropy field (H_k) dependence of frequencies for DJA-ed current amplitudes of 60~120 mA and dotted box corresponding to highest ratio at 20 MHz. After annealing, all curves of H_k nearly show staircase-like enhancment with frequency increase. This is due to their enhancement of eddy current damping, which means it needs more external magnetic field energy to make domain wall motion and domain rotation. With the annealing current density increasing, the variation trend of H_k gradually improve. For 60 mA

annealing stage, the curve of H_k keeps unchanged compared with as-cast state. When at the annealing current increase to 80 and 100 mA, H_k can observably improve in full selected frequency and reach to 1.1 Oe at 20 MHz. Then continue to increase annealing current density, the H_k will show slight fluctuation, but it nearly reaches a saturation value. Accordingly, the definition of the mentioned weak field detection sensor working range (including frequency and magnetic field) means large $[\Delta Z/Z_0]_{max}$ and ξ_{max} and small H_k, at relatively low frequency, especially DJA-ed wire (80 mA, as defined by Eq. 1) with significantly larger $[\Delta Z/Z_0]_{max}$ and ξ_{max} and relatively smaller H_k at 12~20 MHz, which will more suitable and favorable for the practical sensor application especially for weak magnetic field detection owing to the small biased magnetic field and power loss.

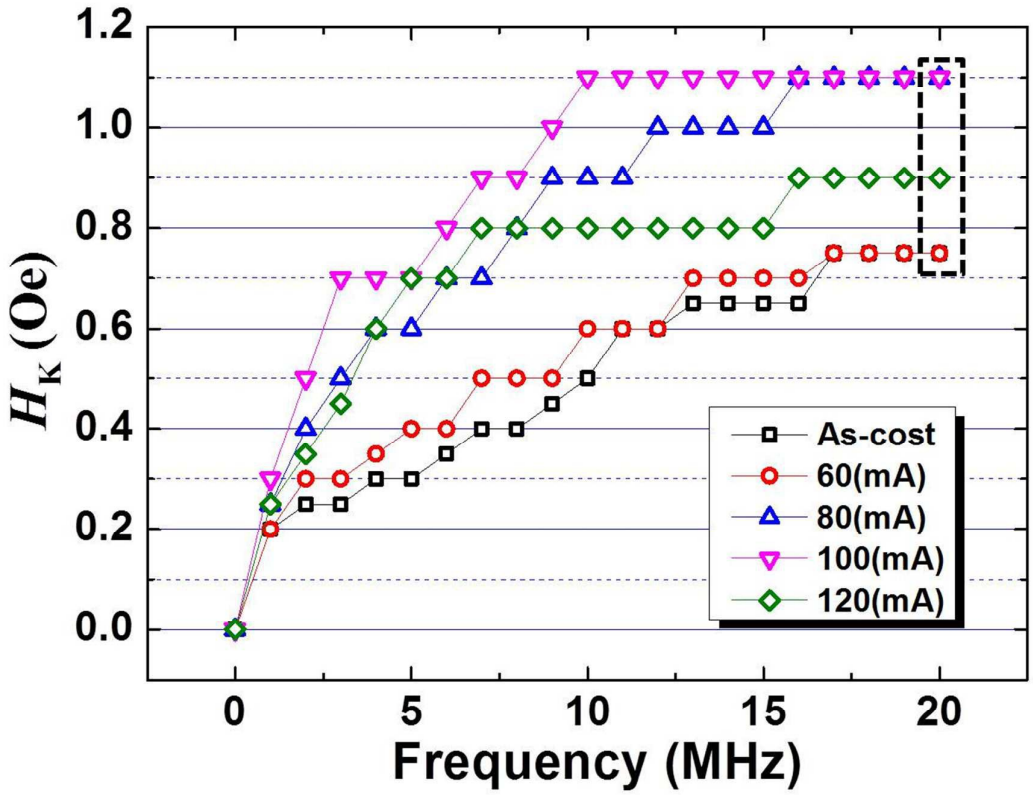

Fig. 6 Statistic diagram of equivalent anisotropy field H_k dependence of frequencies under

different annealing current amplitudes of DJA and the dotted box corresponding to highest ratio at 20 MHz.

Fig. 7 displays the longitudinal magnetic hysteresis (*M*–*H*) loops of as-cast and DJA-ed (as denoted the annealing at 80 mA for 600s) Co-based microwires and the inset shows the image at magnified central area. Both as-cast and DJA-ed microwires exhibit typical features of magnetic bistability with nearly negligible hysteresis. And the magnetizations achieved their saturation state at relatively low external magnetic field. It also indicates almost a reduction trend of the longitudinal saturation magnetization M_s and longitudinal permeability after DJA treatment (M_s decreases from 67.32 emu·g^{-1} of as-fabricated to 61.66 emu·g^{-1} of DJA-ed wire), also the hysteresis narrows down as displayed in inset of Fig. 7. Negative near zero magnetostriction coefficient of Co-based amorphous microwires own axial (or longitudinal) and circumferential direction magnetic domain strutctures.[25,26] The volume fraction of circumferential magnetic domain increases owing to circumferential magnetic field generated by annealing current. Accordingly, volume fraction of axial magnetic domain decreases synchronously. Herein, it can also improve that the circumferential anisotropy further increased the H_k and reduce included angle between axial direction of magnetization and circumferential (Ψ).[27] Structural relaxation and releasing of residual internal stress can effectively recede the coercivity (H_c) thus further to form narrow hysteresis loops.[28] H_k raise the difficulty of easy axis magnetization then cause lower longitudinal permeability. In conclusion,

these changes of magnetic properties induced by DJA show the improvement of the GMI performances.

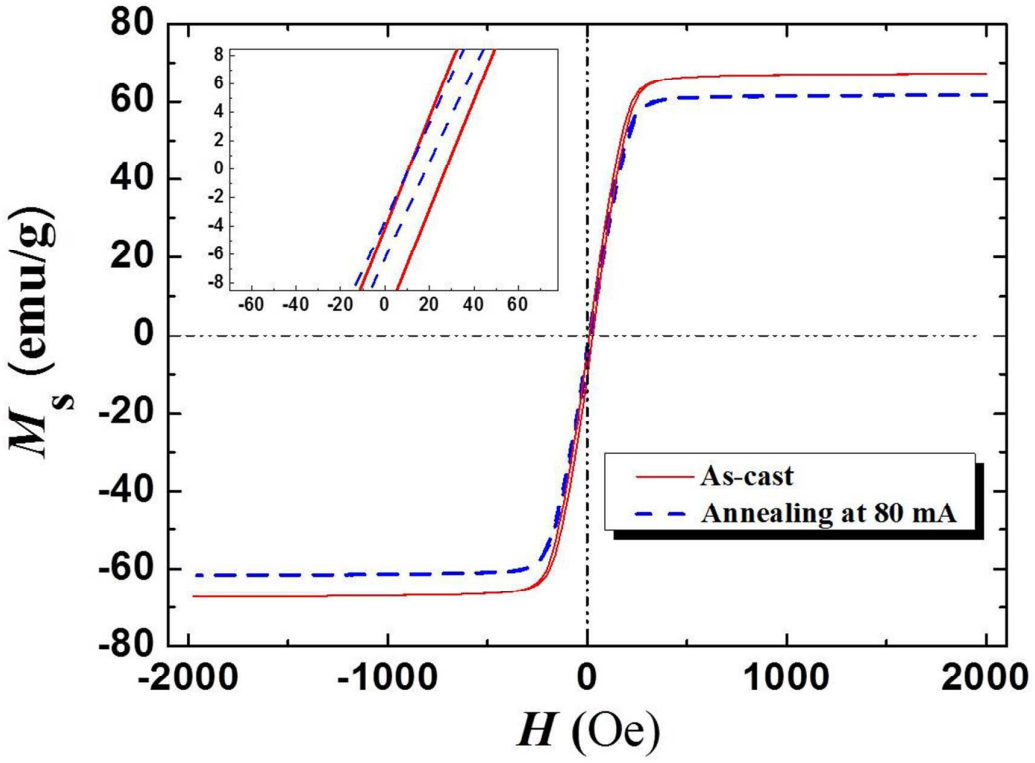

Fig. 7 Magnetic hysteresis (*M–H*) loops and magnified central region of as-cast and 80 mA DJA-ed microwires in inset.

In microstructural perspective and the previous work,[29] magnetic properties are closely related to the microstructure of amorphous microwires. The high-resolution transmission electron microscopy (HRTEM) analyses and selected area electron diffraction (SAED) were employed to investigate the microstructure of as-cast and DJA-ed wires. Inverse fast Fourier transform (IFFT) and autocorrelation function (ACF) method are applied for providing more directive evidence to establish the corresponding relationship between microstructure variation and GMI effect. Fig. 8 displays the HRTEM images and SAED of the studied microwire and the

corresponding local magnification. SAED pattern of DJA-ed microwire (Fig. 8e) displays crystalline diffraction light-spots and SAED image of as-cast microwire (Fig. 8b) only present classic amorphous diffraction rings, which indicate the presence of large amount of nanocrystalline. Generally, ACF technique with reference of microstructural information was applied to quantitatively identify and calculate the degree of nanocrystallization on the selected micro area of as-cast and DJA-ed microwires.[30] Detailed process of the ACF technique includes the following several steps: Firstly, HRTEM image was divided into 64 sub-images with the uniform area of 18 nm^2, e.g. one sub-image with coordinates of (→5, ↓6) in Fig. 8c, which express distinct crystal-like diffraction fringes in ACF patterns, was chosen as a reference pattern to depict the nanocrystallization in this research work. Next, other sub-images whose ACF sub-images exhibit clearer and more uniform fringes than the reference pattern were considered as being nanocrystalline. Statistical analysis of all small select areas reveals the degree of nanocrystallization in Figs. 8(a) and (d) are 6.25% and 32.81%, respectively. Nanocrystals appearing on the amorphous matrix in as-cast microwires which may be induced during the process of fabrication and the degree is relative to the technological parameters.[31] Comparative study IFFT of region 1#, 2# in (b) and 3#, 4# in (e), the arranged atomic micro-regions change more regular.[22] Apparently, DJA treatment has a remarkable enhancement in the degree of nanocrystallization. Formation of nanocrystalline (in terms of the degrees of nanocrystallization by ACF technique) owe to the diffusion and rearrangement of atoms which were induced by the co-actions of thermal activation energy and circular

magnetic-field energy during DJA process. And DJA can both release inner residual stress and improve structural relaxation properly. Well known, Joule-heat treatment will reduce the concentration of free volume and defects further to properly reduce the magnetoelastic coupling effect, thus enhances the permeability (it also named as circumferential permeability) which can improve the GMI effect. In addition, it also can effectively regulate the distribution of circular magnetic anisotropy domain, which is considered as the reason of self-generated external circular magnetic field during annealing process.[14] Meanwhile the release of inner residual stress and relatively higher nanocrystallization degree can obliviously reduce the resistivity of DJA-ed microwires, which is another important influence factor of GMI effect.

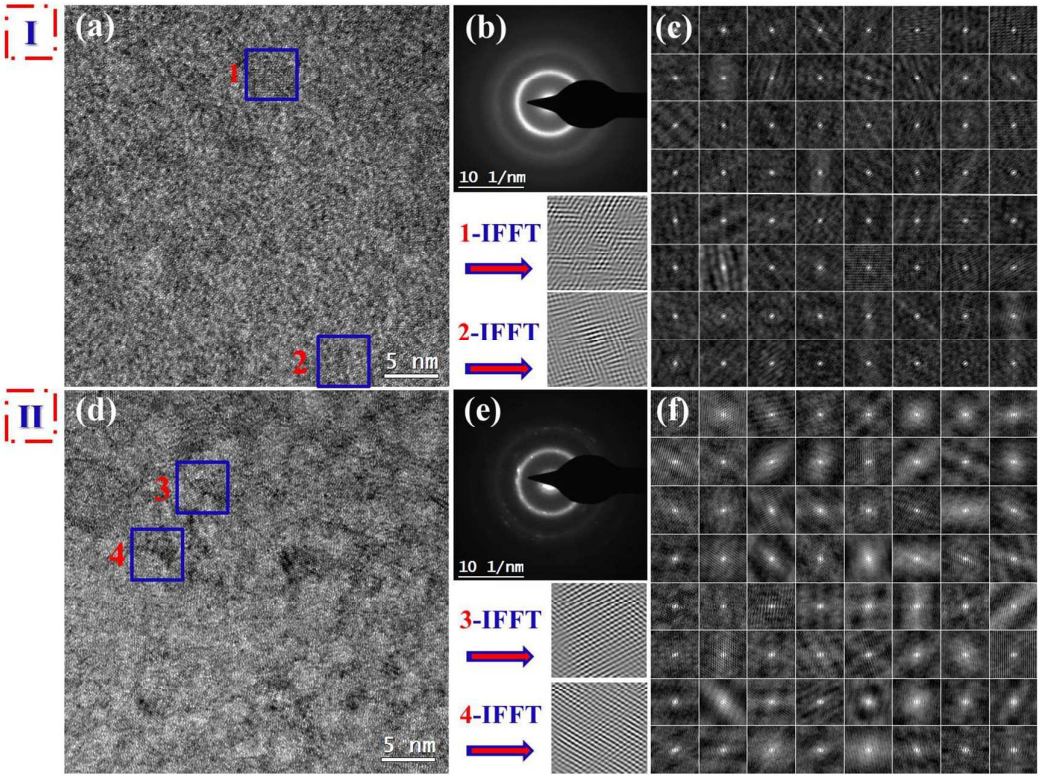

Fig. 8 HRTEM images of the as-cast (a) and DJA-ed 80 mA (d) amorphous microwire with nanocrystalline (region 1#, 2#, 3#, 4#). (b) and (e) SAED of the corresponding whole areas; the

two lower picture severally show inverse fast Fourier transform (IFFT) patterns of area 1#, 2# in blue frame in (a) and 3#, 4# in (d). (c) and (f) express the autocorrelation function (ACF) of HRTEM images.

Fig. 9 illustrates the impendences at different external magnetic fields (H_{ex}=0, H_{ex}=100 Oe, H_{ex}= H_k), resistance (R_0) and reactance (X_0) separation of Z_0 (Fig. 9b). Inset of Fig. 9b shows the DC resistivity (ρ_{dc}, at room temperature) dependence with annealing current value at 20 MHz. We indicated that the Z_0 decline with annealing stage then increase after threshold value (corresponding to 80 mA) while the Z_{max} essentially constant, but the Z_{H_k} shows as slightly increasing then sharply reduced. Maximum value of $\Delta[Z-Z_0]$ and $\Delta[Z-Z_{max}]$ respectively reach at 80 mA and 60 mA annealing stage then decrease gradually as shown in Fig. 9a. The R_0 and X_0 separation of Z_0 (Fig. 9b) and DC resistivity (inset of Fig. 9b) curves show the same trend with Z_0. Most of previous current annealed research focus on enhancement of GMI effect owe to the change of Z_{H_k}, however, herein we attempt to analyze a more important influence which is the variation of Z_0. Based on Maxwell equation and ignore Landau-Lifshitz, in amorphous microwire, Z can be expressed by:[15]

$$Z = \frac{l}{2\pi r}\left(\rho_{dc} f \mu_{\varphi}\right)^{1/2} \frac{J_0(kr)}{J_1(kr)}(1+i) \tag{5}$$

where ρ_{dc} is the DC resistivity, J_o and J_1 are Bessel functions, r the wire radius, and μ_{φ} the total permeability for the circumferential direction φ.

Actually，Z_0 means the impendence of alternating current access microwire without H_{ex}. So, it is only related to circumferential magnetization process induced by AC without the axial magnetization. And the change of R_0 is more intense and show

higher value than X_0 as shown in Fig. 9b. Obviously, variation trend of the resistivity ρ_{dc} induced by DJA become the mainly decisive factor for Z_0 value. The releasing of inner residual stress induces the structural relaxation and increases the degree of nanocrystallization during annealing process; these factors decide the trend of ρ_{dc}. At annealed stage of appearance of nanocrystalline (as seen in Fig. 8e), ρ_{dc} will show irreversible break-down.[32] According to the generalized Ziman theory by Nagel about liquid metal, electron scattering mainly depends on relative location of first peak between Fermi surface and structure factor. Disorder structure of amorphous alloy is center of electron scattering, for the structural relaxation and nanocrystalline generated by DJA can effectively decline ρ_{dc}. But with the accumulation of DJA (maybe more than the threshold), then ρ_{dc} visibly increase. Based on different mechanism of scattering, there are two types for resistance of material: one is phonon scattering induced by thermal vibration of lattice atom, this resistance usually associated with temperature (ρ_t); another is scattering perspective of flaw, it will not change with practical temperature, and the temperature coefficient of resistance (TCR) owns small value.[33] We hold the opinion that dispersion of nano crystallization phase will enhance the TCR and increase quantity of heat eddying effect, then the co-action improves the ρ_{dc} at 20 mA AC of impedance tests. In the meantime, three-dimensional nanocrystalline growth will change the stress state of microwire, which can further to increase the ρ_{dc} at room temperature. Variation tendency of Z_{max} and Z_{H_k} is decided by dynamic axial magnetization process, so circumferential permeability can be as the major influenced factor. At $H_{ex} = H_k$, domain wall movement and domain rotation

together determine the μ_φ and then get the largest value. But with the H_{ex} continuously increasing (which is bigger than H_k), the axial direction is hard magnetization direction for circumferential magnetic domain, so the domain rotation is gradually inhibited. When the H_{ex} increases to 100 Oe, domain basically does not rotation which means that μ_φ almost invariant even after DJA treatment. Therefore the tendency of Z_{max} owns a small change as shown in Fig. 9a. For the stage of DJA (both including 60 and 80mA), at beginning the value of μ_φ enhanced slightly, then declined with annealing current increase. The larger nanocrystalline will generate nail-sticked for movement of domain wall and strengthen eddy current damping further to decline the μ_φ. Above all these make the curve of Z_{H_k} just like as shown in Fig. 9a.

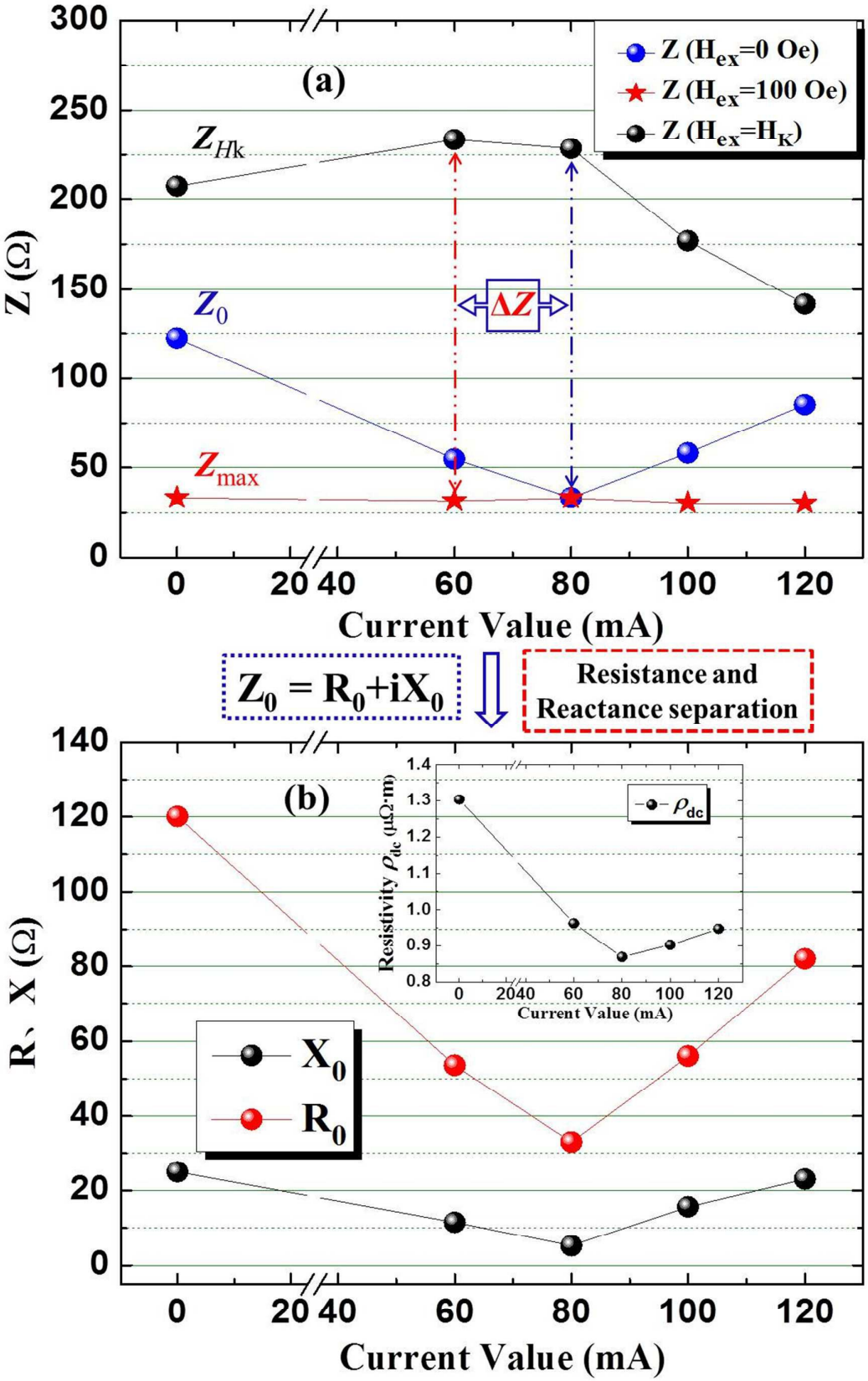

Fig. 9 (a) Impendences at different external magnetic field (H_{ex}=0, H_{ex}=100 Oe, H_{ex}= H_k), (b)

resistance, R_0, and reactance, X_0, separation of Z_0, inset of (b) shows the DC resistivity dependence with annealing current value at 20 MHz.

Overall, through quantitative description of impendence for as-cast and DJA microwires we demonstrate the different mechanism of effect on two GMI definitions. Such different mechanism of DJA post-treatment can be concluded as follows: the enhancement of $\Delta[Z-Z_0]/Z_0$ is resulting from the Z_0 markedly decline and improvement of Z_{Hk}; and $\Delta[Z-Z_{max}]/Z_{max}$ only depends on increase of Z_{H_k}. DJA treatment play a more effective role for the enhancement of $\Delta[Z-Z_0]/Z_0$ in compared with $\Delta[Z-Z_{max}]/Z_{max}$. GMI effect defined by Z_{max} enhance slightly, but it is displays excellent $\xi_{Z_{max}}$ than ξ_{Z_0}. So we can choose the most fitting definition mode for practical application for magnetic sensors and provide novel design ideas.

4. Conclusions

DJA at 60 mA and 80 mA stages have a relatively remarkable effect on the GMI effect: Both two mainly different indexes $[\Delta Z/Z_{max}]_{max}$ and $[\Delta Z/Z_0]_{max}$ increase to 639.13% and 582.59%, and the maximun values of $\xi_{Z_{max}}$ and ξ_{Z_0} increase to 2927.9%/Oe and 1346.4%/Oe, respectively. Meanwhile, the MFS enhance to 1.1 Oe at 20 MHz. Overall, through quantitative description of impendence for the as-cast and DJA microwires we demonstrate the different effect mechanism on two GMI definitions. Therefore, DJA can be used to enhance the GMI effect of amorphous microwires for high-performance sensor applications. In conclusion, we can choose different annealing stage and their corresponding definition mode as the basis according to the practical working environment for designing GMI sensor reasonablely.

Acknowledgements

This work was financially supported by the National Natural Science Foundation of China (NSFC) under grant Nos. 51371067. J.S.L. acknowledges National Natural Science Foundation of China (NSFC) under grant Nos. 51401111 and 51561026, Natural Science Foundation of Inner Mongolia Autonomous Region of China under grant Nos. 2014BS0503.

References

1 M. H. Phan, H. X. Peng, Giant magnetoimpedance materials: Fundamentals and applications, Progress in Materials Science, 2008, **53**, 323–420.

2 M. Knobel, K. R. Pirota, Giant magnetoimpedance: concepts and recent progress, Journal of Magnetism and Magnetic Materials, 2002, **242**(1), 33–40.

3 J. S. Liu, J. F. Sun, D. W. Xing, X. Xue, S. L. Zhang, H. Wang, X. D. Wang, Experimental study on the effect of wire bonding by Cu electroplating on GMI stability of Co-based amorphous wires, Physica Status Solidi A. 2011, **208**, 530–534.

4 H. Chiriac, M. Tibu, V. Dobrea, Magnetic properties of amorphous wires with different diameters, Journal of Magnetism and Magnetic Materials, 2005, **290**(2), 1142–1145.

5 P. Ciureanu, I. Khalil, L. G. C. Melo, P. Rudkowskib, A. Yelona. Stress-induced asymmetric magneto-impedance in melt-extracted Co-rich amorphous wires. Journal of Magnetism and Magnetic Materials, 2002, **249**, 305–309.

6 F. X. Qin，Y. Quéré，C. Brosseau，H. Wang，J. S. Liu，J. F. Sun，H. X. Peng, Two-peak Feature of the Permittivity Spectra of Ferromagnetic Microwire/Rubber Composites, Applied Physics Letters, 2013, **102**, 122903.

7 H. Wang, F. X. Qin, D. W. Xing, F. Y. Cao, H. X. Peng, J. F. Sun. Fabrication and Characterization of Nano/Amorphous Dual-phase Finemet Microwires. Materials Science and Engineering B, 2013, **178**(20), 1483–1490.

8 R. Varga, Y. Kostyk, A. Zhukov, M. Vázquez, Single domain wall dynamics in thin magnetic wires, Journal of Non-Crystalline Solids, 2008, **354**, 5101–5103.

9 V. Zhukova, A. Zhukov, K. García, V. Kraposhind, A. Prokoshind, J. Gonzaleza, M. Vázquez, Magnetic properties and GMI of soft melt-extracted magnetic amorphous fibers, Sensors and Actuators A-Physical, 2003, **106**, 225–229.

10 M. Vázquez, Soft magnetic wires, Physica B-Condensed Matter, 2001, **299**, 302–313.

11 H. Chiriac, T. A. Óvári, Novel trends in the study of magnetically soft Co-based amorphous glass-coated wires, Journal of Magnetism and Magnetic Materials, 2011, **323**, 2929–2940.

12 F. X. Qin，J. Tang，V. V. Popov，J. S. Liu，H. X. Peng，Brosseau C. Influence of Direct Bias Current on the Electromagnetic Properties of Melt-extracted Microwires and Their Composites, Applied Physics Letters, 2014,

104(1), 012901.

13 J. F. Hu, H. W. Qin, F. Zhang, R. K. Zheng, Diameter dependence of the giant magnetoimpedance in hard-drawn CoFeSiB amorphous wires, Journal of Applied Physics, 2002, **91**, 7418–7420.

14 J. S. Liu, F. X. Qin, D. M. Chen, H. X. Shen, H. Wang, D. W. Xing, M. H. Phan, J. F. Sun, Combined Current-Modulation Annealing Induced Enhancement of Giant Magnetoimpedance Effect of Co-rich Amorphous Microwires, Journal of Applied Physics, 2014, **115**(17), 17A326.

15 V. Panina, K. Mohri, Effect of magnetic structure on giant magneto-impedance in Co-rich amorphous alloys, Journal of Magnetism and Magnetic Materials, 1996, **157/158**, 137–140.

16 C. Moron, A. Garcia, Giant magneto-impedance in nanocrystalline glass-covered microwires, Journal of Magnetism and Magnetic Materials, 2005, **290**, 1085–1088.

17 X. Z. Zhou, G. H. Tu, H. Kunkel, G. Williams, Effect of Joule-heating annealing conditions on giant magnetoimpedance of Co-rich amorphous ribbons, Sensors and Actuators A-Physical, 2006, **125**, 387–392.

18 V. Zhukova, A. F. Cobeño, A. Zhukov, J. M. Blanco, S. Puerta, J. Gonzalez, M. Vázquez, Tailoring of magnetic properties of glass-coated microwires by current annealing, Joumal of Non-Crystalline Solids, 2001, **287**, 31–36.

19 K. R. Pirota, L. Kraus, H. Chiriac, M. Knobel, Magnetic properties and giant magnetoimpedance in a CoFeSiB glass-covered microwire, Journal of Magnetism and Magnetic Materials, 2000, **221**, 243–247.

20 S. D. Jiang, D. W. Xing, J. S. Liu, H. X. Shen , D. M. Chen, W. B. Fang, J. F. Sun, Influence of microstructure evolution on GMI properties and magnetic domains of melt-extracted Zr-doped amorphous wires with accumulated DC annealing, Journal of Alloys and Compounds, 2015, **644**, 180–185.

21 H. Wang, F. X. Qin, D. W. Xing, F. Y. Cao, X. D. Wang, H. X. Peng, J. F. Sun, Relating Residual Stress and Microstructure to Mechanical and Giant Magneto-impedance Properties in Cold-drawn Co-based Amorphous Microwires, Acta Materialia, 2012, **60**(15), 5425–5436.

22 J. S. Liu, F. Y. Cao, D. W. Xing, L. Y. Zhang, F. X. Qin, H. X. Peng, X. Xue, J. F. Sun, Enhancing GMI Properties of Melt-extracted Co-based Amorphous Wires by Twin-zone Joule Annealing, Journal of Alloys and Compounds, 2012, **541**, 215–221.

23 J. S. Liu，J. F. Sun，D. W. Xing，X. Xue, Comparative Study on Microstructure and Magnetic properties of Amorphous Wires with Different Diameters, Materials Technology, 2012, **27**(1), 142–144.

23 D. M. Chen, D. W. Xing, F. X. Qin, J. S. Liu, H. X. Shen, H. X. Peng, H. Wang, J. F. Sun. Cryogenic Joule annealing induced large magnetic field response of Co-based microwires for giant magneto-impedance sensor

applications, Journal of Applied Physics, 2014, **116**, 053907.

24 D. M. Chen，D. W. Xing，F. X. Qin，J. S. Liu，H. Wang，X. D. Wang，J. F. Sun, Correlation of Magnetic Domains, Microstructure and GMI Effect of Joule-annealed Melt-extracted Co68.15Fe4.35Si12.25B13.75 -Nb1Cu0.5 Microwires for Double Functional Sensors, Physica Status Solidi A, 2013, **210**(11), 2515–2520.

25 L. V. Panina, K. Mohri, K. Bushida and M. Noda, Giant magneto-impedance and magneto-inductive effects in amorphous alloys (invited), Journal of Applied Physics, 1994, **76**, 6198.

26 M. Vazquez, A. Hernando, A soft magnetic wire for sensor applications, Journal of Physics D-applied Physics, 1996, **29**, 939–949.

27 M. Takajo, J. Yamasaki, F. B. Humphrey, Domain observations of Fe and Co based amorphous wires, IEEE Transactions on Magnetics, 1993, **29**, 3484–3486.

28 K. Mohri, Fdlow, K. Bushida, M. Noda, H. Yoshida, L. V. Panina, T. Uchiyama, Magneto-Impedance Element, IEEE Transactions on Magnetics, 1995, **31**, 2455–2460.

29 H. X. Peng, F. X. Qin, M. H. Phan, J. Tang, L. V. Panina, M. Ipatov, V. Zhukova, A. Zhukov, J. Gonzalez, Co-based magnetic microwire and field-tunable multifunctional macro-composites, Joumal of Non-Crystalline Solids, 2009, **355**, 1380–1386.

30 J. S. Liu, H. X. Shen, D. W. Xing, J. F. Sun, Optimization of GMI properties by AC Joule annealing in melt-extracted Co-rich amorphous wires for sensor applications, Physica Status Solidi A. 2014, **211**(7), 1577–1582.

31 F. X. Qin, Y. Quéré, C. Brosseau, H. Wang, J. S. Liu, J. F. Sun, and H. X. Peng, Two-peak feature of the permittivity spectra of ferromagnetic microwire/rubber composites, Applied Physics Letters, 2013, **102**, 122903.

32 N. Banerjee, R. Roy, A. K. Majumdar, Electrical resistivity in the $Fe_{100-x}B_x$ series ($13 \leq x \leq 26$), Physical. Review. B, 1981, **24**, 6801–6806.

33 P. Peng, R. S. Liu, Q. Quan, The effect of high content of metalloid on resistivity and temperature coefficient of resistivity of amorphous TM-M alloys, Materials Science and Engineering B, 1996, **38**, 62–64.